A new measurement of the interplanetary hydrogen density with ALAE/ATLAS 1

Eric Quémerais, Jean-Loup Bertaux, B. R. Sandel, Rosine Lallement

Astron. Astrophys. 290, 941–955 (1994)

ASTRONOMY AND ASTROPHYSICS

A new measurement of the interplanetary hydrogen density with ALAE/ATLAS 1

Eric Quémerais[1,2], Jean-Loup Bertaux[1], Bill R. Sandel[2], and Rosine Lallement[1]

[1] Service d'aéronomie du CNRS, BP 3, 91371, Verrières le Buisson, France
[2] Lunar and Planetary Laboratory, University of Arizona, 901 Gould-Simpson Building, Tucson, AZ 85721, USA

Received 21 January 1994 / Accepted 17 May 1994

Abstract. The ALAE Lyman α spectrophotometer has been flown on the ATLAS 1 mission aboard the space shuttle Atlantis from March 24 until April 2, 1992. During this mission, when the cargo bay of the shuttle was pointing toward the zenith, observations of the interplanetary Lyman α glow were made possible with the help of a hydrogen absorption cell that absorbed most of the geocoronal emission. Here, we analyze these zenith data. The calibration factor of the instrument has been determined by studying the full geocoronal emission seen at the zenith. Intercomparison of radiative transfer calculations of both the interplanetary and geocoronal Lyman α emissions allows for a precise determination of the interplanetary hydrogen density. This estimate is independent of the value of the solar Lyman α flux at line center for the time of observation. The hydrogen number density obtained here is 0.15 ± 0.05 cm^{-3}. Using solar wind ion flux measurements available from the NSSDC database to estimate the ionization rate of neutral hydrogen, we find a more accurate value equal to 0.165 ± 0.035 cm^{-3}. Previous measurements obtained from other space experiments are also reviewed. Those obtained independently of solar flux/calibration factor cluster in the range 0.11-0.17 cm^{-3}, which is nearly a factor of two higher than most previous estimates. This is mainly due to the use of an incorrect ionization rate for neutral hydrogen in earlier works. This relatively high number density is a further indication that the heliospheric shock, compressed by the interstellar flow, might be nearer than previously estimated.

Key words: interplanetary Lyman α – interplanetary medium – interstellar wind

1. Introduction

The Atmospheric Lyman Alpha Emission experiment (ALAE) has flown aboard the space shuttle Atlantis from March 24 to April 2, 1992. As part of the ATLAS 1 mission, the primary scientific objectives of this experiment are to study Lyman α emissions from deuterium and hydrogen atoms in the upper mesosphere and in the thermosphere. However, by looking at the zenith it has been possible to measure the extraterrestrial Lyman α emission that arises from interplanetary neutral hydrogen atoms resonantly scattering the solar Lyman α photons.

The interplanetary origin of this Lyman α glow, which adds to the geocoronal Lyman α emission seen from an altitude of 300 km, has first been identified as such by two different experiments aboard the OGO 5 satellite in 1969 (Bertaux & Blamont 1971; Thomas & Krassa 1971). This radiation is due to resonance scattering of the solar Lyman α photons (121.6 nm) by the neutral hydrogen atoms present in the interplanetary medium. These atoms, which come from the interstellar medium, interact with the solar environment when reaching the inner part of the heliosphere.

Owing to the motion of the Sun relative to the local interstellar cloud, the neutral interstellar hydrogen atoms are not at rest in the solar frame of reference. As shown by various authors (e.g. Thomas 1978 and references therein), this leads to an interstellar wind of neutral atoms which penetrate deep inside the solar system. At large distances where it is not affected by the Sun, this wind can be characterized by a bulk velocity vector and a temperature. On the other hand, the collisionless flow of neutral hydrogen inside the heliosphere is strongly affected in the neighborhood of the sun (less than about 30 astronomical units). There, they feel the opposing effects of Lyman α radiation pressure and gravitational attraction by the sun. Neutral hydrogen atoms are also strongly ionized when they are close to the Sun. This ionization is due to photo-ionization by solar EUV photons ($\lambda < 91.2$ nm) and also to resonance charge exchange with solar wind protons, the latter contributing to roughly 80% of the total. This leads to the so-called ionization cavity around the Sun (see Lallement et al. 1985). In a first approximation, when solar ionizing fluxes are assumed spherically symmetric, the distribution of neutral hydrogen is axisymmetric and the ionization cavity is elongated in the direction of the flow.

It has been shown that when the effects of the coupling between the interstellar neutral atoms and the interstellar and solar

Send offprint requests to: Eric Quémerais

plasmas at the heliopause are neglected, the neutral hydrogen distribution in the inner heliosphere is well represented by a stationary model characterized by two solar and three interstellar parameters (Thomas 1978; Lallement et al. 1985). In what follows, we will refer to this model as the *hot model*. A precise determination of the three interstellar parameters (number density, bulk velocity and temperature in the interstellar medium) is necessary if we wish to represent correctly this phenomenon. Measurements of the interplanetary Lyman α emission line profile obtained with a hydrogen absorption cell on board *Prognoz* 5/6 (Lallement & Bertaux 1984; Bertaux et al. 1985) have yielded a good estimate of the bulk velocity (20 ± 1 km/s) and temperature (8000 ± 1000 K) of the interplanetary flow. On the other hand, the value of the number density of neutral hydrogen in the interstellar medium is still a matter for discussion.

Since the beginning of the 1970's, many space experiments have studied the interplanetary Lyman α glow (see Ajello et al. 1987). Yet, the estimates of the interstellar density parameter vary greatly from study to study, ranging between 0.03 and 0.3 cm^{-3} (see Sect. 7 for a review of previous measurements). This wide span is due to the various problems inherent to this kind of study. The first difficulty to take into account is the calibration of the instruments. Once they are in space, it is often difficult to estimate absolute calibrations and changes in the calibration factors after launch, thus leading to large uncertainties. Furthermore, since a direct measurement is not possible, all derived densities are model dependent. Yet, it has been shown that radiative transfer effects have often been underestimated in the past. Even in the inner heliosphere where ionization effects due to the Sun destroy most the neutral hydrogen, it is necessary to take multiple scattering into account (Quémerais & Bertaux 1993). Another uncertainty is due to the variation of the illuminating flux itself, because the solar Lyman α absolute flux is rather poorly known at line center. Most of the systematic measurements correspond to the integrated solar line, whereas only the line center excites the resonance of H atoms. Finally, it is likely that coupling effects at the heliopause interface lead to discrepancies between the hot model and actual hydrogen distributions in the heliosphere. However, recent studies by Baranov & Malama (1993) or Osterbart & Fahr (1992) show that the hydrogen distribution in the inner heliosphere is mainly dependent on solar parameters because of the predominance of the ionization processes in this region of the heliosphere. Then, the main discrepancy which appears in that case when compared to a hot model is a filtration effect of the neutral hydrogen atoms at heliopause crossing. Seen from Earth, the hydrogen distribution is equivalent to a hot model, though in that case the number density D_∞ inferred by the study of the Lyman α glow pattern corresponds to the interstellar wind parameters *after* heliopause crossing, which can differ from the value in the interstellar medium before going through the terminal structure of the expanding solar wind plasma. This fact can be extremely important for the study of the heliospheric interface but has little direct consequence for the present study of the ALAE data set.

In this paper, we analyze the ALAE/ATLAS 1 data to get a new estimate of the interstellar neutral hydrogen density D_∞ obtained in an absolute manner, independent of the calibration factor of the instrument and of the exact value of the illuminating solar flux. The principle of the method is quite simple. With the same instrument (ALAE) we compare the emissions from two clouds of atomic hydrogen that are illuminated by the same solar flux: one is the interplanetary cloud (whose number density we seek) and the other is the geocorona, where the H density is well known and documented by many previous atmospheric studies.

After a presentation of the data set in the next section, we explain how the geocoronal Lyman α emission has been used to estimate the calibration factor of the instrument and then has been removed from the measured signal. For the method applied here, it is not necessary to know the actual value of the illuminating flux at Lyman α line center. The data are then compared to a full radiative transfer model of the interplanetary Lyman α glow as established by Quémerais & Bertaux (1993). The value of 0.165 ± 0.035 cm^{-3} found here is consistent with a previous measurement made in 1983 with a similar instrument on Spacelab 1.

In Sect. 7, we have compared this value to many previous Lyman α determinations of D_∞. Four other determinations, also independent of absolute calibration, cluster in the range 0.11-0.17 cm^{-3}, which is about a factor of 2 higher than density estimates published in the 70's. However, when these previous observations are re-analysed, starting from quoted intensities, but compared with our hot model, they yield densities which are revised upward, mainly because of a new estimate of the lifetime T_d of an H atom versus ionization.

This relatively high value of D_∞ is a further indication that the heliospheric shock may be nearer than previously estimated. Indeed, a greater dynamic pressure for the interstellar flow will push the equilibrium surface between solar and interstellar winds closer to the Sun. And, as shown by Baranov & Malama (1993), the component of the dynamic pressure along the wind axis due to neutral-plasma coupling may be an important factor, especially if there is a high H number density in the interstellar medium.

2. ALAE zenith observations

As part of the ATLAS 1 mission, the ALAE experiment was primarily dedicated to the study of deuterium and hydrogen atoms in the upper mesosphere and in the thermosphere. This instrument contains one hydrogen cell and one deuterium cell which are used alternatively or together to characterize the geocoronal deuterium and hydrogen Lyman α emissions (Bertaux et al. 1992).

ALAE is basically a spectrophotometer containing a spherical holographic grating of 15 cm diameter. The entrance aperture of the spectrometer (a circular hole defining a field of view of 3° diameter) is at the focus of a parabolic off-axis mirror, which can be rotated step by step to scan the FOV in one plane. On this mirror, the angle between incidence and reflection is 90°. The exit hole of the spectrometer admits a bandwidth of about 50 Å around Lyman α and rejects the strong 1304 Å dayglow of atomic oxygen. The deuterium absorption cell, located behind

the spectrometer, has figured windows of MgF_2 that image the exit hole of the spectrometer on the MgF_2 window of a photomultiplier (type 641-G side window) of exceptionally high quantum efficiency (28%), used in a pulse counting mode (integration time equal to 0.4 s). The hydrogen absorption cell is in front of the entrance of the spectrometer (see Fig. 3 in Bertaux et al. 1992).

The instrument is mounted in the cargo bay so that the rotation axis of the scan mirror is parallel to the X axis(long axis of the shuttle), allowing the line of sight of ALAE to scan in the YZ plane of the shuttle. The total FOV which can be explored with the mirror is limited by a stray light baffle, over a range of $\approx 130°$ extending from 30° on the left of the -Z axis (pointing outside from the cargo bay, perpendicular to the XY plane of the wings) to 10° below the +Y axis (Fig. 1a).

The performance of ALAE on ATLAS 1 was far superior to that on Spacelab 1, first because the ATLAS 1 orbit was more favorable for deuterium observations, and second because the instrument sensitivity was much larger (by a factor of 37, as indicated later). Preliminary results concerning ALAE observations of deuterium in the mesosphere and lower thermosphere have been reported (Bertaux et al. 1992).

The hydrogen absorption cell allowed us once more to study the interplanetary Lyman α emission by pointing the line of sight at the zenith. In this configuration, most of the geocoronal emission can be absorbed because there is no Doppler shift between the H cell and the geocorona. This observation required a special attitude of the shuttle with its cargo bay toward the sky. During the ten days of the ATLAS 1 mission, we had seven opportunities for zenith observations. Each observation period lasted roughly one shuttle orbit (90 minutes). The X axis of the shuttle was aligned with the velocity vector VV (in fact, -VV) and the -Z axis was toward the local zenith. As a result, the line of sight of the instrument was perpendicular to the velocity vector of the shuttle, thus ensuring that most of the geocoronal emission was absorbed by the hydrogen cell. Whatever the direction of the line of sight, it was always kept in the ZY plane.

Figure 1a shows the orbital configuration and the possible scan angle at two positions along the orbit. The solar zenith angle varied along the orbit between 40° and 140°. Figure 1b shows the position of the Earth at the time of the ATLAS 1 and Spacelab 1 missions, in respect to the direction of the interstellar wind direction. The maximum interplanetary emission is near the upwind direction and Fig. 1b shows that ALAE observes this direction in the second half of the night along the orbit during ATLAS 1.

In Fig. 2, we show the path of a typical mirror scan during one zenith session. It was obtained with a special program of commands to the scan mirror, established during the mission with the knowledge of the actual orbit after launch. During the 40 minutes shown, a wide range of the sky is scanned and the line of sight goes from downwind to upwind regions as the shuttle goes from the dayside to the nightside of its orbit. We have also shown the trace on the celestial sphere of the plane perpendicular to the vector corresponding to the difference between the interstellar wind velocity and the Earth orbital velocity. For the

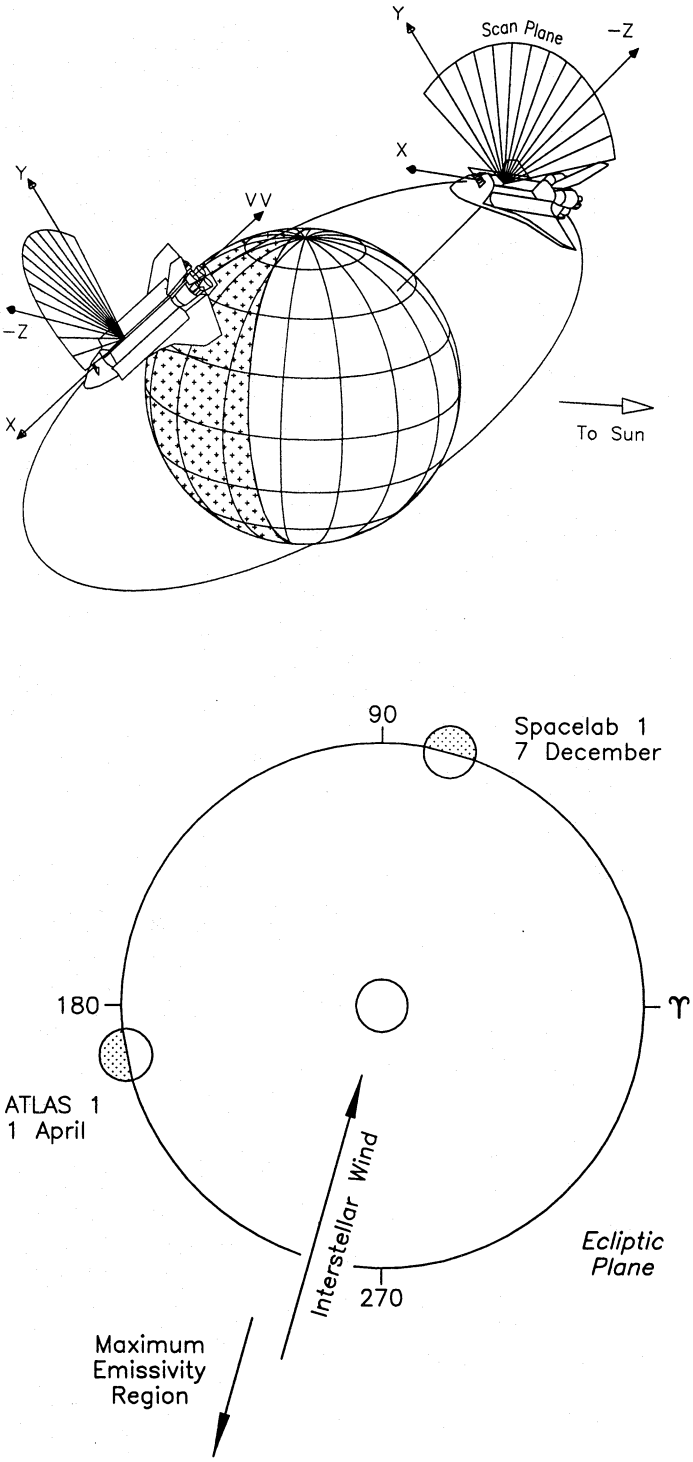

Fig. 1. The upper graph is a representation of the orbital configuration and the possible scan angle at two positions along the orbit. The orbital plane makes an angle of 57° with the equatorial plane, and the solar zenith angle varies between 40° and 140°. The -Z axis defines the direction of the cargo bay of the shuttle. The lower graph represents the various ecliptic longitudes at the time of observation. The interplanetary emission is higher near the upwind direction (254°), i.e. on the nightside of the Earth at 190°

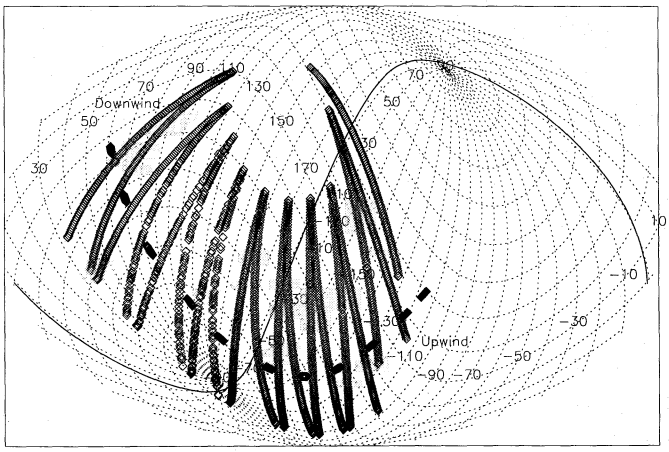

Fig. 2. Path of a typical zenith scan (here session Z711) performed during one shuttle orbit. Here, only half of the orbit is shown. The ecliptic latitude of the line of sight vector is plotted as a function of its ecliptic longitude. The direction of the origin of the interstellar wind (upwind direction) and the direction of the flow (downwind direction) have been added. The intersection of the plane perpendicular to the interstellar wind velocity vector with the celestial sphere is represented by the line. For lines of sight in this plane, there is no Doppler shift between the interplanetary emission and the hydrogen cell which means that the interplanetary Lyman α emission is partially absorbed when the cell is activated

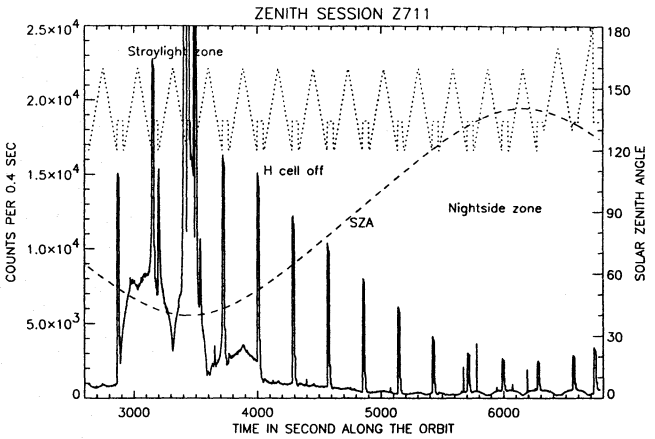

Fig. 3. Representation of the raw signal (counts per 0.4 second) measured for session Z711, performed during one shuttle orbit on April 1, 1992. The data are plotted as a function of time (seconds since 0 GMT, day 92) along the orbit. As time increases, the shuttle goes from the dayside to the night side (the solar zenith angle, on the right hand scale, increases). On the dayside where the geocoronal emission is highest (minimum solar zenith angle is 40°), a third component, related to the instrument mirror position, appears clearly. The small regularly spaced peaks correspond to the unabsorbed geocoronal emission, when the H cell is off. These values are used for calibration purposes. Otherwise, the H cell is activated at a high level of absorption.The dotted line represents the mirror position in the shuttle YZ plane during the celestial sphere scan. This plot emphasizes the correlation between the mirror position and the stray light on the dayside

directions of sight inside this plane (Zero Doppler Shift Circle, Bertaux & Lallement 1984), there is no Doppler shift between the H cell and the interplanetary atoms scattering the Lyman α photons. The shuttle orbital velocity is not considered here because the line of sight is perpendicular to the VV axis. Then the H cell absorbs the maximum amount possible of both the interplanetary and geocoronal emissions. For directions outside this plane, only the geocoronal signal is absorbed which makes a study of the interplanetary Lyman α emission possible, even from the relatively low altitude of the shuttle (300 km).

Owing to the geometry of the shuttle orbit, the solar zenith angle ranged between 40° and 140°. So, on the dayside of the orbit, the geocoronal emission amounts to about 20 kiloRayleigh and to about 4 kiloRayleigh on the nightside. When the H cell is activated, the remaining dayside and nightside geocoronal emissions are about 1 kiloRayleigh and 200 Rayleigh respectively (see Fig. 3). These values should be compared to the value of the interplanetary Lyman α emission. A rough estimate based on the analysis in this paper gives about 900 Rayleigh in the upwind direction and 300 Rayleigh in the downwind direction. Then this study was made possible because, for certain lines of sight, the geocoronal emission was nearly totally absorbed by the H cell while the interplanetary emission was not. In addition, the time of year of the observation was near optimal. Indeed, when the nightside of the Earth corresponds with the upwind direction the interplanetary emission is best seen because it is then 4 times larger than the remaining non-absorbed geocoronal signal. This ideal period corresponds to the beginning of June (the ecliptic longitude of the upwind direction is 254°). On the other hand, to achieve a maximum Doppler shift between the geocoronal hydrogen and the interplanetary hydrogen atoms, the Earth's ecliptic longitude should be as close to 164° (beginning of March) as possible, which minimizes the width of the sky zone along the Zero Doppler Shift plane where the interplanetary signal will be absorbed by the H cell. Then, the ATLAS 1 mission at the end of March 1992 was near optimum for study of interplanetary H.

On the other hand, the previous observation with the same instrument on Spacelab 1 (Bertaux et al. 1989) was much less favorable. This mission was in December 1983, at a time of year when the upwind direction corresponds with the Earth's dayside (Fig. 1), and the shuttle orbit was always close to the terminator thus causing a high geocoronal signal throughout the orbit. In Sect. 4, we will compare the two results obtained in 1983 and 1992.

Unfortunately, a full study of the seven ATLAS 1 zenith observation sessions has not been possible. Unexpectedly, a stray light emission was observed on all the sessions during the dayside part of the orbit. Its origin could not be ascertained though it was clearly correlated with the times when the shuttle cargo bay was directly lit by the sun and some sunlight was entering deeply in the ALAE baffle. However for solar zenith angles larger than 50°, this unwanted signal was absent and we can measure the interplanetary emission. In Fig. 3, we have plotted the raw data as a function of time along the orbit. The stray light, which is correlated with the instrument mirror position, is

present between 3000 and 4000 s, that is when the solar zenith angle is below 52°.

After 4000 s, there is no stray light and the signal is due to the added contributions of the interplanetary emission and the geocoronal emission. At regular intervals (about every 285 s), the H absorption cell was turned off for a short time (about 25 s) and the line of sight directed toward the zenith. These observations appear as large peaks, as compared to the situation when the H cell is on, in which case most of the geocoronal emission is absorbed, and the remaining signal is composed of the geocoronal signal I_{gON} not absorbed by the H cell, and the interplanetary signal I_{pON}. Occasionally a star crosses the FOV, detected as a narrow spike (for instance, at t = 6200 s). Except for these spikes (and for times of stray light), the measured signal I_{ON} can be written as

$$\begin{aligned} I_{OFF} &= I_g + I_p \\ I_{ON} &= I_{gON} + I_{pON} \\ I_{ON} &= R_g \cdot I_g + R_p \cdot I_p \end{aligned}$$

where R_g and R_p are reduction factors for the geocoronal and the interplanetary signals when the H cell is on. The absorption power of the H cell can be controlled by running more or less electrical current inside the tungsten filament, which breaks H_2 molecules into atoms. For this particular session, a power level labelled H46 was used, producing a Lyα absorption width of 65 mÅ (FWHM). Some technical characteristics for various power levels of the H cell are given in Table A1 of Bertaux et al. (1989).

The difference $I_{OFF} - I_{ON}$ is mainly due to the absorption of the geocoronal signal by the H cell. Clearly from Fig. 3 the amplitude of this geocoronal contribution is correlated to the SZA, as expected for zenith observations from 300 km altitude.

In Fig. 4, the same data are plotted on a smaller scale. Here, only the part corresponding to the night side of the orbit is shown (time after than 4000 s). The data when the H cell is off, used for calibration purposes (see next section), have been removed. Therefore, the signal is composed only of I_{gON} and I_{pON}. The following exercise will be to separate the contributions of both emissions.

A certain number of interesting features appear on this plot. First, as time increases, the solar zenith angle increases also. It means that, on a timescale of one shuttle orbit, the absorbed geocoronal signal is going toward its nighttime minimum. Yet, after time 5000 s, the total signal is globally increasing on the same timescale, except for strong regularly spaced intensity dips on a smaller scale of about 200 s. This overall increase is attributed to I_{pON} variations when going toward the upwind hemisphere maximum interplanetary emission. The directions of sight plotted for various times in Fig. 2 correspond to the same segment of time. On this plot, we see also that on 10 occasions the scan crosses the zero Doppler line on the sky for which the interplanetary Lyman α emission is strongly absorbed. This explains the strong intensity dips on the shorter timescale shown by the data, since for each scan one goes from a totally unabsorbed interplanetary signal to a partially absorbed one. It is interesting to note that if the unabsorbed signal gives us a measurement of the hydrogen density in the interplanetary medium, on the other hand the absorption features are sensitive to the velocity distribution of these interplanetary H atoms.

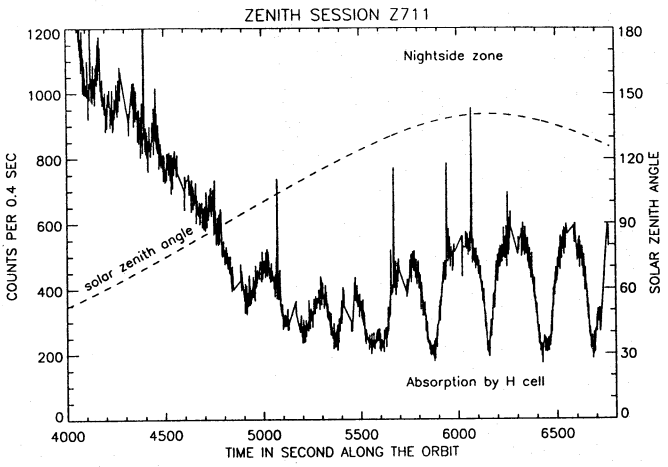

Fig. 4. Representation of the raw signal (counts per 0.4 second) of session Z711 when the H cell is activated (level 46). There are two scales of variation in the data. The first is of the order of 200 s and is due to the absorption of interplanetary Lyα depending on the scan geometry shown in Fig. 2. It corresponds to the difference between the absorbed and unabsorbed signals. The second, of the order of one orbit, corresponds to the increase of the interplanetary emission as the shuttle goes from the downwind to the upwind hemisphere (solar zenith angle increase shown by dotted line). On the same time scale, the absorbed geocoronal signal decreases because the solar zenith angle is increasing

As a conclusion of this section, it can be stated that the geocoronal signal I_{gON} dominates in the first half of Fig. 4, whereas the interplanetary signal I_{pON} dominates in the second half. However, we have still the task to determine the contribution of I_{gON} where I_{pON} dominates, in order to achieve a better accuracy on the retrieval of I_p and on the interplanetary density D_∞.

3. Estimate of the calibration factor

As pointed out above, our determination of the interplanetary hydrogen density number depends on our knowledge of the calibration factor of the ALAE instrument. We have used here a method developed by Bertaux et al. (1989) which takes advantage of the unabsorbed geocoronal emission I_g. In Fig. 3, we see that the hydrogen cell was regularly shut off to measure the full zenith geocoronal emission for various values of the solar zenith angle.

From the shuttle altitude (300 km) and looking upward, the hydrogen atoms on the line of sight follow a distribution which depends mainly on the density n_{ex} and temperature T_{ex} at the exobase just above the shuttle (Bertaux 1974). The exobase, at an altitude of roughly 500 km, is the point of the atmosphere above which the hydrogen atoms follow collisionless ballistic trajectories. Each H atom higher in the atmosphere can be traced back to the intersection of its trajectory with the exobase. As pointed out in Bertaux et al. (1989), at the shuttle altitude and for a zenith direction of sight the atoms contributing to the

emission mainly originate from the same region of the exobase just above the shuttle. The hydrogen distribution can be characterized for a given number density and temperature at the exobase with the formalism developed by Chamberlain (1963), in the simple case where n_{ex} and T_{ex} are uniform all over the Earth (spherical H distribution). When n_{ex} and T_{ex} vary (with SZA, for example), one can still compute numerically the exospheric H distribution by taking into account atoms which come from all the points of the exobase. However, Vidal-Madjar and Bertaux (1972) have shown that, up to an altitude of $\approx$ 3000 km, the vertical distribution above a given point of the exobase is mostly dictated by the local values of n_{ex} and T_{ex}. Since this is also true below the exobase, the vertical line of sight contains atoms of local origin, determined by n_{ex} and T_{ex} at the shuttle coordinates.

In order to determine the calibration factor, the geocoronal intensity data (in counts per 0.4 s) must be compared to the result of a model of radiative transfer in the geocorona. Spherically symmetric density distributions reflecting the correct local distribution parameters at the exobase and the radiative transfer model described by Thomas (1963) and Bertaux (1974) have been used to estimate the intensity I_g measured along the orbit.

As can be seen in Fig. 3, there is a strong variation of the signal between dayside and nightside, roughly a factor of 5. This is not only due to the variation of the solar zenith angle, but also to temperature and density variations with the local time at the point of observation (see e.g. Hedin 1983). Unfortunately our radiative transfer model can be applied only to isothermal spherically symmetric H density distributions. However, since most of the intensity comes from below 3000 km altitude, and since the H distribution below 3000 km along a vertical reflects the local exobase conditions n_{ex} and T_{ex}, we will assume that a good approximation for the zenith intensity in a non-uniform exosphere consists of computing the intensity in a spherically symmetric model determined by n_{ex} and T_{ex}, the local conditions.

The data have been compared with the results of our radiative transfer model for various spherically symmetric H density distributions with reasonable exospheric density and temperature parameters (Fig. 5). The model results were then interpolated according to the variation of the local temperature and density as a function of the solar zenith angle. The temperature and density variations were obtained by use of the semi-empirical MSIS model (Hedin 1983) which takes into account solar activity. The exospheric temperature was assumed between 1000 and 1400 K and density at the exobase was between 3 and 6×10^4 cm^{-3} to cover the range of values given by the MSIS model on the date of observation (April 1, 1992) and along the ATLANTIS orbit, as a function of latitude and local time. In Fig. 5 we have plotted the data to model ratio, in counts per 0.4 s per Rayleigh, as a function of solar zenith angle (SZA), for various interpolations inside the grid of spherically symmetric models. All lines (except the solid one) are for a constant value of n_{ex} along the orbit, but with the value of T_{ex} predicted by the MSIS model (T_{ex} interpolation inside the various isothermal models). For a given spherically symmetric model, the intensity is roughly

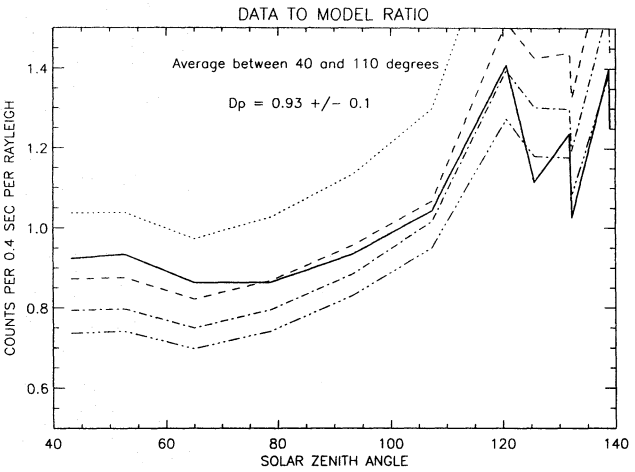

Fig. 5. Data to model ratio for the geocoronal zenith intensity seen from the shuttle altitude of 300 km. A rough estimate of the interplanetary emission has been subtracted from the data (see text). The geocoronal models were computed for various solar zenith angles assuming spherically symmetric density distributions. The H distributions in the geocorona are characterized by the temperature and number density at the exobase (500 km). The exospheric temperature for each solar zenith angle was obtained from the MSIS model using the solar indices at the time of observation. Each line corresponds to one exobase density value. The thick line has been interpolated in the results of various models following the density prediction of the MSIS model for the actual solar parameters at the time and position of observation. The dotted line is for $n_{ex} = 3 \times 10^4$ cm^{-3} at the exobase. The dashed line is for $n_{ex} = 4 \times 10^4$ cm^{-3}, the dash-dot line is for $n_{ex} = 5 \times 10^4$ cm^{-3} and the dash-dot-dot line is for $n_{ex} = 6 \times 10^4$ cm^{-3}

proportional to the scale height of the atmosphere and so is proportional to the temperature. The solid line is then obtained by interpolation between the constant density models, for the value n_{ex} predicted by MSIS along the orbit. Before commenting on Fig. 5, we note that, in order to evaluate correctly the data to model ratio, the contribution of the interplanetary emission had to be subtracted from the data. Here, only a rough estimate is necessary because this contribution is small. In Fig. 4 it appears that the maximum interplanetary emission seen on the nightside corresponds to about 500 counts per 0.4 sec. We have then computed the interplanetary emission seen for the various lines of sight used here and for a given set of parameters (interstellar parameters 8000 K and 20 km/s, solar parameters $\mu = 1$ and $T_d = 1.2 \times 10^6$ s). Then its maximum was scaled to fit the 500 counts per 0.4 sec. These values were then subtracted from the data with no H cell absorption before computing the data to model ratios plotted in Fig. 5.

For a solar zenith angle larger than 110°, it appears that our models, interpolated in temperature with the results of the MSIS model, do not match the data well. The most obvious possibility is that the approximation by a spherical geocoronal model based on local conditions is invalid at large solar zenith angles. Indeed, in the night side, the foot of the line of sight is no longer illuminated by the sun. The shadow height increases with SZA, and the atoms which are directly illuminated, and which

contribute to a large part of the signal, are at a high altitude and come from all the regions of the exobase. The nightside data represent more an average of exobase conditions than the model which represents local conditions, and therefore the nightside intensities are larger than predicted by the model, as indicated by Fig. 5.

All the models were computed assuming an arbitrary reference value for the solar Lyman α flux at line center F_o equal to 2.5×10^{11} cm^{-2} s^{-1} Å^{-1}. All modeled intensities are proportional to this assumed value. In fact, our real interest is not in the calibration factor. The knowledge of the actual Lyman α flux at line center is not necessary here. We are really interested in the coefficient which expresses the relation between the data and our model. If we call A_p the calibration factor in units of Rayleighs for 1 count per counting time of 0.4 s, we have the relation

$$I_{F_s} = A_p \cdot C \tag{1}$$

where C represents the signal in counts per 0.4 second and I_{F_s} the actual intensity in Rayleigh. F_s is the Lyman α flux at line center at the time of observation. But using the proportionality to the flux at line center, we have

$$C = A_p^{-1} \cdot \left(\frac{F_s}{F_o}\right) \cdot I_{F_o} = D_p \cdot I_{F_o} \tag{2}$$

The calibration factor A_p is intrinsic to the instrument, whereas the coefficient D_p varies with time like F_s, to which it is related. Yet, over one orbit, F_s variations are certainly very small and D_p may be assumed constant. By comparing the geocoronal intensity measured with the H cell off toward zenith at various places along the orbit to the geocoronal model prediction with F_o, a series of data to model ratios are obtained, (solid line in Fig. 4), each of them being an estimate of D_p (Eq. 2). The actual counting rate measured for the interplanetary emission, divided by D_p, gives an intensity (in Rayleigh units) which is then compared to a model of interplanetary Lyman α intensity computed for the same F_o and various hydrogen densities. The true density at infinity D_∞ is the one which gives a computed model intensity equal to the measured one. Therefore D_∞ is determined without knowledge of the actual value of the solar flux F_s. For session Z711 on April 1, 1992 shown in Fig. 5 and limiting the average of D_p to a SZA value less than 110°, we find

$D_p = 0.93 \pm 0.1$ counts per 0.4 second per Rayleigh

The fact that the solid line representing the data to model ratio is pretty constant below SZA=110° indicates that both the MSIS semi-empirical model of H atmospheric distribution and our radiative transfer approach are valid. The true instrument calibration factor A_p, not necessary here, is then given by $F_s/((D_p \cdot F_o)$.

So, to estimate the number density in the interplanetary medium, without knowing the actual value of the illuminating solar Lyman α flux at line center, it is possible to use instead the hydrogen density distribution in the geocorona as a reference. Of course, the value of reference, i.e. the number density of H atoms at the exobase, influences this estimate. Yet, since the medium is optically thick, the dependence on the exobase density is not as large as it would be in an optically thin case.

As seen in Fig. 5, doubling the density from 3×10^4 to 6×10^4 cm^{-3} at the exobase, and therefore at all altitudes along the line of sight increases the model intensity by only $\approx 40\%$. A given difference between the MSIS model prediction and the actual exospheric density produces a smaller error in the calibration factor and in the following estimate of D_∞.

4. Modeling the interplanetary Lyman α glow

It has been shown by various authors (e.g. Thomas 1978; Lallement et al. 1985), that the density distribution of neutral hydrogen in the interplanetary medium is not homogeneous. Near the Sun where ionization effects by EUV photons and solar wind protons are important, the region where there is no neutral hydrogen is called the ionization cavity. The size and shape of this cavity surrounding the Sun is clearly dependent on the values of the solar EUV photon flux and the solar wind proton flux (Lallement et al. 1985). By assuming a Maxwellian distribution in the interstellar medium (*at infinity*), one can compute the stationary hydrogen distribution at every point of the heliosphere. The result is completely defined by three parameters in the interstellar medium (number density D_∞, bulk velocity V_∞ and temperature T_∞) and two parameters expressing the solar activity.

The focusing parameter μ, is the ratio of the force due to the radiation pressure and the gravitational attraction. When it is larger than 1, the net force on the H atoms is repulsive. On the other hand, it is attractive when it is smaller than 1. According to Lyα solar flux estimates, this parameter may vary between ≈ 0.5 and 1.2 during the solar cycle. As shown by Quémerais (1993), the focusing parameter does not have a strong influence on the H distribution in the upwind hemisphere and the average value of 1 gives a correct estimate of the intensity pattern in the upwind direction. This is not so in the downwind direction where focusing of H atom trajectories may influence the shape of the ionization cavity.

The other solar parameter measures the efficiency of the ionization processes on the neutral hydrogen atoms. Since the solar ionizing fluxes follow a $1/r^2$ dependence, the total ionization rate at distance r from the sun, noted $\beta(r)$, is simply equal to $T_d^{-1}\left(r_o/r\right)^2$ where T_d is the lifetime against ionization at one astronomical unit (r_o is equal to 1 AU). For a stationary model, this last parameter sets the dimension of the ionization cavity. Clearly, the value of the ionization rate influences the Lyman α backscattered intensity pattern, as we discuss in the next section.

Our aim here is to estimate the value of D_∞, that is the number density in the interstellar medium, which is in best agreement with the H distribution as seen from Earth's orbit. Since there is no easy inversion technique for this problem, we have computed the backscattered intensity for various model parameters and compared it to the data. The hydrogen density distributions

used here do not take possible effects of the heliopause interface into account (e.g. Osterbart & Fahr 1992; Baranov & Malama 1993). Indeed, the existence and effects of the heliospheric interface are still matters for discussion. There could be no effect on neutral hydrogen at all. Besides, in the works mentioned above, it appears that within about 30 AU of the sun, the distribution of neutral hydrogen is fixed by the solar parameters. All the emission seen from 1 AU comes from this region of the heliosphere (Quémerais & Bertaux 1993). Then by using a standard hot model to study the ALAE zenith data, we may not be studying the actual interstellar parameters, that is those that apply before crossing the heliosphere interface structure, but rather the post-shock parameters imprinted on the H atoms distribution at the heliopause. Then, if there is a filtration of neutral atoms at the heliopause, the value D_∞ found here is only a fraction of the actual value in the interstellar medium and refers rather to the interplanetary H number density at 50-60 AU in the upwind direction.

To compute the backscattered intensity seen from Earth, it is necessary to take multiple scattering effects into account. Though the ionization cavity is an optically thin medium, the fact that it is surrounded by an optically thicker medium precludes using the optically thin approximation here (Quémerais & Bertaux 1993). For instance, various authors analyzing space data (Bertaux et al. 1985; Lallement et al. 1991) have overestimated the value of T_d, the H lifetime against ionization at 1 AU because the optically thin approximation tends to underestimate the intensity backscattered from the cavity. This leads to an underestimate of the actual size of the ionization cavity and then of the ionization rate itself. By reanalysing the Prognoz 5/6 and inner heliosphere Voyager 1/2 data, Quémerais & Bertaux (1993), using a radiative transfer calculation of the Lyman α interplanetary glow, have shown that the value of T_d was closer to 1.2×10^6 s rather than the 2×10^6 s obtained with the optically thin approximation for the considered periods of observation. During a solar cycle, the value of T_d may vary between 10^6 and 1.5×10^6 s according to measurements of solar wind proton fluxes. In fact, the value assumed for T_d will have a direct effect on the value of D_∞ inferred from the ALAE data. Taking as a reference the distribution obtained with $T_d = 1.2 \times 10^6$ s, we have compared the upwind intensities obtained by our radiative transfer calculation for session Z711 both for 1.5×10^6 s and 10^6 s. It appeared that, for values of D_∞ between 0.1 and 0.25 cm^{-3}, the first case always led to intensities higher than the reference by 25% and the second one smaller by 15%. This effect is quite important and will be accounted for in the uncertainty of the estimate for D_∞ obtained here.

It must be added that the radiative transfer model used here does not take fully into account the phase function for the resonance scattering of Lyman α photons. However, a first step has been taken to correct for this. For each point of the heliosphere, we have evaluated the source function, noted $S(\boldsymbol{r})$, which is the emissivity divided by the Lyman α excitation rate at 1 AU (g_o). This source function can be split between the primary term S_o, which comes directly from the Sun, and a secondary term S_s, due to the influence of all the other points in the heliosphere. We have then assumed that the phase function is washed out for the secondary term since secondary photons come from all over space. In that respect, the backscattered intensity seen at position $\boldsymbol{r}$ for a line of sight defined by $\boldsymbol{\Omega}$ is given by

$$I(\boldsymbol{r}, \boldsymbol{\Omega}) = \frac{g_o}{4\pi} \int_0^{+\infty} S(\boldsymbol{r} + s\boldsymbol{\Omega})\, T(\tau_o[\boldsymbol{r}, \boldsymbol{r} + s\boldsymbol{\Omega}])\, ds \qquad (3)$$

Here, g_o is the Lyman α excitation rate at 1 AU and is equal to 1.8×10^{-3} s^{-1} for a Lyα line center flux of $F_s = 3.32 \times 10^{11}$ s^{-1} cm^{-2} $Å^{-1}$ (i.e. for $\mu = 1$). The transmission along the line of sight is given by the first Holstein function $T(\tau_o)$ where τ_o is the optical thickness at line center (Thomas 1963; Meier 1991). The phase function is given by $\phi(\gamma)$ where γ is the angle between incoming and outgoing radiation at the point of scattering. Then following our assumptions,

$$\frac{1}{4\pi} S(\boldsymbol{r}) = \frac{\phi(\gamma)}{4\pi} S_o(\boldsymbol{r}) + \frac{1}{4\pi} S_s(\boldsymbol{r}) \qquad (4)$$

The expression (4) is not exact because at 1 AU the H distribution is not homogeneous; rather there is a strongly emissive region (Maximum Emissivity Region) in the upwind hemisphere. Therefore the emission indicatrix before the secondary term should not be strictly isotropic. Further models will treat this problem in a more detailed manner. Otherwise, the photometric models used here are identical to those developed by Quémerais & Bertaux (1993).

Finally the use of a hydrogen cell required that the reduction factor, the fraction of the absorbed intensity divided by the unabsorbed intensity (see Lallement & Bertaux 1984) could be computed to see whether the interplanetary emission was partly absorbed. At the present time, our radiative transfer model is a photometric model and does not allow for a precise computation of the line profiles required to analyze the reduction factor. So to do this, we have used an optically thin approach to model the line profiles which takes the exact H velocity distribution into account (Lallement et al. 1985; Quémerais et al. 1992). We are currently working on a next step to include radiative transfer effects here. However, it must be noted that the reduction factor is used here only to assess the absorption of the interplanetary emission, to ensure that the determination of D_∞ is not affected by the H cell.

5. Data to model comparison

As we pointed out before, the interplanetary Lyman α emission is maximum on the nightside of the shuttle orbit where the geocoronal emission is minimum (see Fig. 6). However to get the best estimate possible for the interplanetary component, the geocoronal signal has been estimated for subtraction in the following manner.

By comparing our geocoronal Lyman α models to the regularly distributed measurements of the geocoronal emission for an unactivated cell during the orbit (Fig. 3), we have been able to obtain a semi-empirical estimate of the geocoronal emission that is more representative than the geocoronal models alone

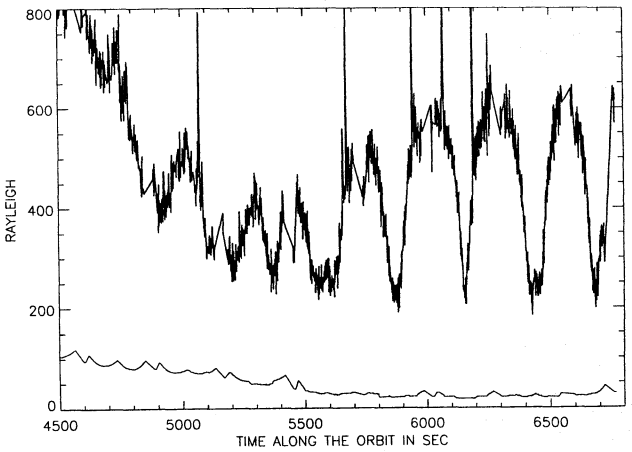

Fig. 6. Representation of the Z711 zenith data as a function of time. Here, we have used the calibration factor for an assumed value of the Lyman α flux at line center equal to 2.5×10^{11} s^{-1} cm^{-2} Å^{-1}. On the same plot we have added the model of remaining geocoronal emission not absorbed by the H cell when it is activated. This curve was obtained from one isothermal spherically symmetric model at 1000 K, which is the minimum value of the exospheric temperature predicted by MSIS for the time of observation. This model was also multiplied by a data-to-model correction factor dependent on the solar zenith angle, as explained in the text

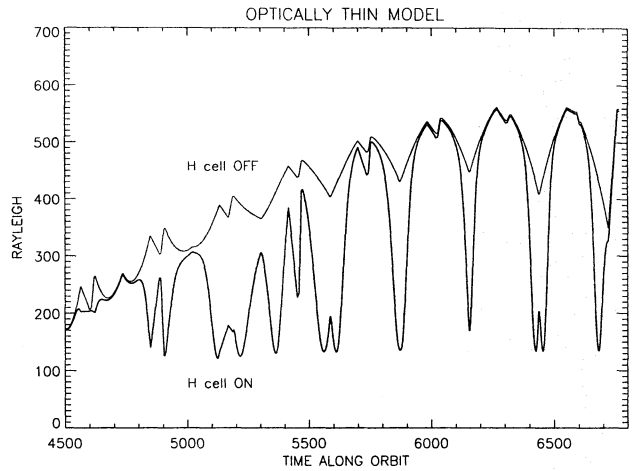

Fig. 7. Optically thin calculation of the absorbed and unabsorbed interplanetary emissions for session Z711. The absorbed emission corresponds to an H cell with optical thickness at line center equal to 1060 and a temperature of 500 K. The curves allow for the determination of the reduction factor as a function of time and show when the interplanetary emission is not absorbed by the cell. The interstellar wind is characterized by a bulk velocity of 20 km/s and a temperature of 8000 K. The solar parameters used for this computation are $\mu = 1$ and $T_d = 1.2 \times 10^6$ s

and that can be used as a correction factor for our models. Our spherically-symmetric models do well represent the variation of intensity as the line of sight scans the celestial sphere. Indeed, when the line of sight is not pointing directly at the zenith the intensity increases because the thickness of the atmosphere along the line of sight increases. However, a correction factor varying with the solar zenith angle is necessary because of the discrepancy between data and model that appears in Fig. 5 for large values of SZA (nightside). To estimate this correction factor for a model with $n_{ex} = 5 \times 10^4$ cm^{-3} and $T_{ex} = 10^3$ K, we have divided the data by the model results obtained when the cell is not activated at the various values of solar zenith angle available. These exobase parameters have been chosen because they correspond to the MSIS estimate obtained on the nightside with the solar parameters corresponding to session Z711. A first order estimate of the interplanetary contribution had been removed (in counts per 0.4 sec) to ensure as much as possible that only emission from the geocorona was taken into account. The simplest approach was to assume that when the H cell is activated, all the signal is due to the interplanetary hydrogen, and then to subtract that value from the unactivated cell data. This implies that we have neglected roughly one percent of the geocoronal signal, that is the value of the reduction factor for a gas at 1000 K and the H cell equivalent width of 65 mÅ. The data-to-model ratio obtained is not constant, as already pointed out in Sect. 3, but depends on the solar zenith angle. In fact, the ratio tends to increase for higher values of the solar zenith angle because the geocorona can not be represented by an isothermal model. Assuming that the geocoronal emission follows the same data-to-model variations as a function of the solar zenith angle when the H cell is activated, we have then multiplied the results of the isothermal model for an activated H cell by the interpolated data-to-model ratio according to the value of the solar zenith angle at the point of observation. Of course, the result is not dependent on the assumed exospheric parameters of the isothermal model used here. The lower curve in Fig. 6 shows the result divided by 0.93 to convert to Rayleigh units, assuming a solar Lyman α flux at line center equal to the reference value F_o.

Here, we must point out that the residual geocoronal emission is correctly represented only on the nightside of the orbit. This appears in Fig. 6 where clearly for times smaller than 5000 s (daytime data) the geocoronal emission is underestimated. For such times the gas is hotter than the assumed 1000 K and consequently the reduction factor (which measures the transmission of the cell not the extinction) is larger than obtained from our isothermal model. However, to estimate the interplanetary hydrogen density, we are interested only in times larger than 6000 s where the assumed value of 1000 K for T_{ex} is representative. Then, the estimate of the residual geocoronal emission has been removed from the data. The resulting values have been used in Figs. 8 to 10.

As we pointed out before, we do not have yet a precise model for the interplanetary Lyman α line shape taking full radiative transfer into account. However, it was necessary to evaluate for each line of sight whether the interplanetary signal was absorbed

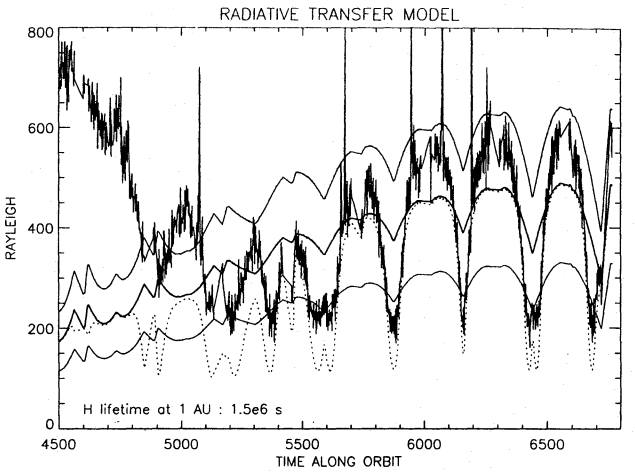

Fig. 8. Data of session Z711 after subtraction of the geocoronal emission. The results of three radiative transfer models are shown assuming a solar flux at line center equal to 2.5×10^{11} s^{-1} cm^{-2} Å^{-1}. The models correspond to $\mu = 1$ and $T_d = 10^6$ s. The lower curve corresponds to $D_\infty = 0.1$ cm^{-3}, the intermediate curve to $D_\infty = 0.15$ cm^{-3} and the upper curve to $D_\infty = 0.2$ cm^{-3}. The dotted line corresponds to the intermediate curve multiplied by the reduction factor computed from an optically thin model of the interplanetary emission with the same parameter values. A best fit is obtained for $D_\infty = 0.18$ cm^{-3}

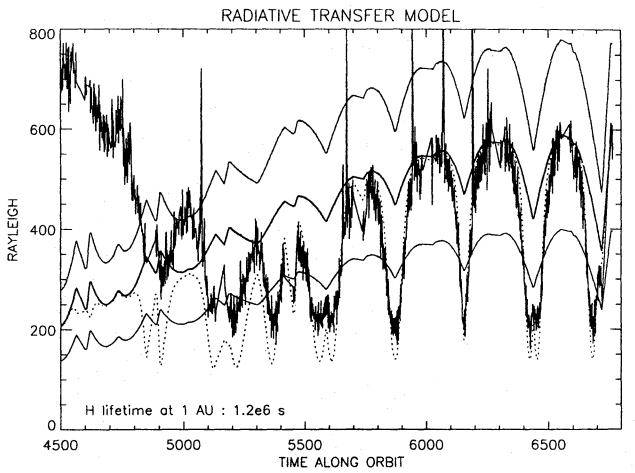

Fig. 9. Same as Fig. 8, but with a value of the H lifetime against ionization at 1 AU equal to 1.2×10^6 s. The best fit is obtained with $D_\infty \approx 0.15$ cm^{-3}

or not, taking the actual parameters of the activated hydrogen cell. This was done with the help of an optically thin model of the line shape used before to study the Prognoz 5/6 Lyman α data (Lallement 1983; Lallement et al. 1985) and which takes the actual hydrogen velocity distribution into account to compute the line shape and the reduction factor. In Fig. 7, we show the resulting predictions of the optically thin model. The reduction factor for the interplanetary emission derived in this way has been used hereafter.

In Figs. 8 to 10, we present the results of our radiative transfer models for three different values of the H lifetime against

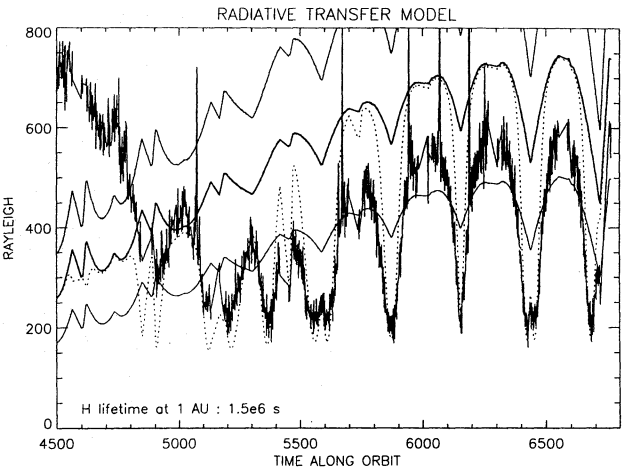

Fig. 10. Same as Fig. 8, but with a value of the H lifetime against ionization at 1 AU equal to 1.5×10^6 s. The best fit is obtained with $D_\infty \approx 0.12$ cm^{-3}

Table 1. Estimates of D_∞ for various T_d.

T_d (s)	1.0×10^6	1.2×10^6	1.5×10^6
D_∞ (cm^{-3})	0.18 ± 0.02	0.15 ± 0.02	0.12 ± 0.02

ionization ($T_d = 10^6$, 1.2×10^6, 1.5×10^6 s) and three values of the interstellar density parameter (0.1, 0.15, 0.2 cm^{-3}). First, the importance of the actual value of the lifetime against ionization appears clearly. In Table 1, the best fit value of D_∞ is given for the various values of T_d. If we choose the mean value of $T_d = 1.2 \times 10^6$ s, we find that D_∞ is 0.15 ± 0.05 cm^{-3}. The uncertainty given here comes from the fact that the uncertainty on the signal shown in Fig. 6 is roughly 50 Rayleigh and comes from the uncertainty on the calibration factor D_p. This is added to the uncertainty on the actual value of T_d at the time of observation.

This estimate can be improved if the value of the H lifetime at one astronomical unit is obtained by a different means. Ajello et al. (1987) and Pryor et al. (1992) have used measurements of solar proton fluxes at 1 AU to estimate the rate of ionization by charge exchange with solar wind protons. Solar wind ion flux and velocity measurements are available from the National Space Science Data Center. We have used these values along with the charge exchange cross section given by Osterbart & Fahr (1992) to compute the ionization rates against charge exchange averaged over a period of one year, which is roughly the time scale for a H atom crossing the near-Sun environment. We have then added an estimate of the ionization rate due to solar EUV flux using the values given by Banks & Kockarts (1973) for various periods of the solar cycle.

The relevant data for the March-April 1992 period have been used to estimate T_d. The value found here is 1.1×10^6 s, corresponding to high solar wind flux events in the ecliptic plane

after the solar maximum. As a consequence of this strong solar activity the estimate of the mean value of T_d is rapidly changing in 1991 and 1992 leading to a large uncertainty. The corresponding value for the previous solar cycle (in 1981) was found to be 1.4×10^6s. The discrepancy may be due to a stronger activity in the equatorial region of the Sun and this may lead us to somewhat overestimate the mean value of the ionization rate. We see from Table 1 that the product $T_d \cdot D_\infty$ is roughly constant at 0.18×10^6 s cm^{-3}. Then, we find that D_∞ is equal to 0.165 ± 0.035 cm^{-3}.

It must be noted also that Table 1 shows that the *upwind* intensity is proportional to $T_d \cdot D_\infty$, in spite of all the complications introduced in the model with ionization and radiative transfer.

6. The Spacelab 1 results

The ALAE instrument had already been flown on the Spacelab 1 mission in December 1983 under the name 1-ESO17, as part of the ESA payload complement. Though the time of observation was not as favorable as in the case of ATLAS 1 (upwind direction close to the dayside and shuttle orbit always close to the terminator), the interplanetary emission was definitely observed (Bertaux et al. 1989).

There are several important differences between the two flights. First, the instrument flown on Spacelab 1 was the Flight Unit #1, (MV1), whereas the instrument flown on ATLAS 1 was the Spare unit (MV2). The calibration factor was determined during the flight by comparison with the geocorona, in an exercise similar to the one presented here (Bertaux et al. 1989). A value of Ap = 39.4 ± 4 Rayleigh/count/0.4 s was found (for $F_s = 2.5 \times 10^{11}$ phot cm^{-2} s^{-1}), to be compared to the ALAE value $D_p^{-1} = 1.075$ R/counts/0.4 s. The ALAE instrument MV2 was 37 times more sensitive than the MV1 during Spacelab 1. We knew from ground calibration measurements that the MV1 integrated on Spacelab 1 was not as good as desirable and 9 months before launch in 1983 we asked to replace the MV1 by the much better spare unit MV2. Unfortunately our request was rejected by the Spacelab 1 Project. Contributing to the low sensitivity of MV1 was a poor grating efficiency of 3%, to be compared to an expected value of 18%, actually achieved for MV2.

A second difference was in the geometry of observations. At the time of Spacelab 1 (December 7, 1983), the Earth was at an ecliptic longitude of 76°, nearly downwind from the Sun, precluding observations near the upwind direction where the interplanetary emission is maximum (Fig. 1). In addition, the Spacelab 1 orbit was near the terminator, the shuttle was always in sunlight. The Solar Zenith Angle varied only between 80 and 100°, to be compared to the maximum SZA value of 140° for ATLAS 1, much deeper on the nightside. As a result, at the position along the orbit at which the interplanetary emission was at its maximum, and when the H absorption cell is activated, the remaining geocoronal intensity (not absorbed) contributed ≈ 50% of the total signal for Spacelab 1, and only ≈ 10% for ATLAS 1 conditions. The subtraction of the geocoronal signal to retrieve the interplanetary emission is therefore more reliable in the present analysis of ATLAS 1 data.

In the 1989 analysis of Spacelab 1 interplanetary data, it was found that a model with $D_\infty = 0.065$ cm^{-3} (which was then a currently admitted value) predicted an intensity substantially lower than the data (Fig. 11, in Bertaux et al. 1989). Since then, important progress has been made in the modeling of the interplanetary intensity (including multiple scattering and reducing the lifetime from $T_d = 2 \times 10^6$ s to more realistic values), and hence we treated again the Spacelab 1 data in the same manner as the one depicted in this paper. The NSSDC solar wind data, used as in the previous paragraph, has yielded a value of T_d equal to 1.2×10^6 s, which is roughly the mean value over a solar cycle.

In Fig. 11, we present the data from Bertaux et al. (1989) along with our radiative transfer models obtained for the three values of D_∞ indicated (0.1, 0.15, 0.2 cm^{-3}). Once again the dotted line corresponds to an optically thin estimate of the reduction factor multiplied by the unabsorbed intensity computed from our radiative transfer model. Though the signal to noise ratio of this first instrument was not as good as achieved in ALAE/ATLAS 1, we obtain an estimate of D_∞ between 0.15 and 0.2 cm^{-3}, which is compatible with the ALAE result. Here, the actual uncertainty due to the geocoronal signal is about 100 Rayleigh because the calibration factor is known within 10 % and the sum of interplanetary and geocoronal emissions amounts to roughly 1000 Rayleigh (Bertaux et al. 1989). In such a case, the data shown in Fig. 11 are marginally compatible with values of D_∞ between 0.1 and 0.24 cm^{-3}. Assuming that the ionization parameter is correctly estimated by the use of the NSSDC data, we find that D_∞ is equal to 0.17 ± 0.07 cm^{-3}.

However, as emphasized above, the conditions of observation were much better for ATLAS 1 than for Spacelab 1, and the ATLAS 1 estimate is therefore much more reliable.

Adjustment of the actual calibration factor of ALAE

The calibration factor of ALAE/ATLAS 1 derived in Section 3 was derived from a comparison with a geocoronal model prediction using a reference solar flux $F_o = 2.5 \times 10^{11}$ photon cm^{-2} s^{-1} Å^{-1} at line center. At the time of ALAE measurements, there were no measurements of solar flux at line center. However, the integrated solar Lyα flux F_{tot} can be estimated from its established correlations with other solar parameters. According to the HeI equivalent width of the solar line at 10830 Å (Lean 1990), this flux is estimated to be 3.7×10^{11} photon cm^{-2} s^{-1} for April 1 1992. The usual assumption that F_s (in photon cm^{-2} s^{-1} Å^{-1}) is numerically equal to F_{tot} (in photon cm^{-2} s^{-1}) was recently confirmed from IUE high resolution spectra of the solar Lyα line reflected from the moon with no interference from the geocoronal absorption (Widemann, private communication). Therefore, the actual calibration factor of ALAE should rather be $A_p = F_s \cdot (F_o D_p)^{-1}$ or $A_p = 1.48 \times 1.75 = 1.59$ Rayleigh per count per 0.4 s. Accordingly, all intensities quoted in Rayleigh unit in this paper from ALAE/ATLAS 1 measurements should be multiplied by $F_s/F_o = 1.48$. In particular, the

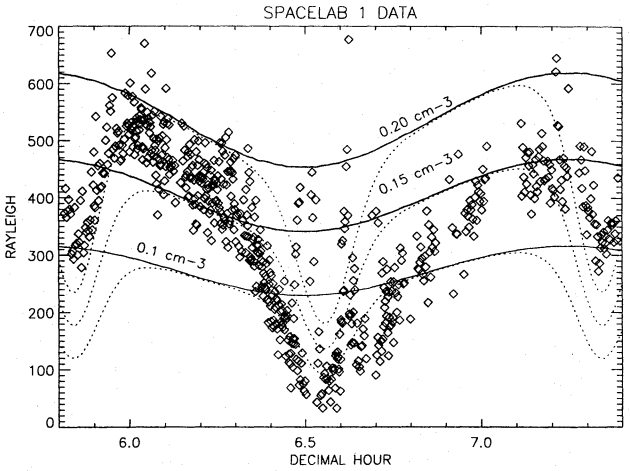

Fig. 11. H Lyman α brightness measured by Spacelab 1 as a function of time (see Bertaux et al. 1989). On the same plot we have added the model results obtained for the parameters indicated in the text. The best fit is obtained for $D_\infty = 0.17 \pm 0.03$ cm^{-3}. For these observations, the mirror was not moved and as a consequence there are only two absorption minima, where the orbital plane crossed the Zero Doppler Shift Circle

maximum interplanetary emission in the upwind direction is found to be $600 \times 1.48 = 890$ R. Of course, this adjustment has no influence at all on the determination of D_∞. Also, it could be noted that the actual ratio of sensitivities between ATLAS 1 and Spacelab 1 should take into account the real solar fluxes at both epochs, rather than the reference value F_o which yielded a ratio of 37. The resulting ratio of solar fluxes equal to 3.7/3.1 yields a ratio of sensitivities equal to 31.

7. Comparison with previous determinations

In Table 2 are listed the previous measurements which can be (and in almost all cases have been) used to derive the interstellar neutral H density inside the heliosphere. They cover different kinds of Lyman α observations by a variety of instruments, plus the more recent measurement of H^+ pick-up ions on board Ulysses (Gloeckler et al. 1993). In the third column is indicated either the published intensity in the region of maximum emission, near the upwind direction, or the density derived from this intensity. In such a case, the lifetime T_d of an H atom at 1 AU which was used by the authors to derive the density from the intensity is indicated in column 4.

In addition, in order to eliminate some scatter due to the use of different model parameters by the various authors, we performed the following exercise. Starting from the initially published Lyα intensity values, we re-estimated D_∞ according to the geometry, the solar conditions during the measurements, and our standard hot model, in a uniform and consistent manner.

First, we used fixed interstellar parameters (velocity at 20 km/s, temperature of 8000 K), whereas some authors had taken sometimes slightly different values of 22 or 26 km/s, or 10000 K. Second, we used a uniform method to estimate the solar Lyman α line center flux, by using the solar He 1083 nm line width as a proxy (Lean 1990). For data prior to 1975, a correlation with the calcium plage index data was used (Ajello et al. 1987). This is needed for estimating both the exciting solar Flux F_s at the time of the measurements and the radiation pressure to gravity ratio, the μ parameter. Third and most important, we have discarded observations obtained in the downwind region, and a mean value of 1.2×10^6 s for the lifetime T_d of an H atom at 1 AU was selected when no more accurate estimate was available. The results are shown in Table 3.

Indeed, observations near the upwind region (maximum of intensity) are much more safely interpreted than observations in the downwind region. One reason is that, near the upwind region, the intensity is linearly related to lifetime T_d, and depends only moderately on the radiation pressure characterized by the focusing parameter μ, and the radiative transfer effects add only a few percent to the intensity (Quémerais & Bertaux 1993). On the contrary, in the downwind region, the density distribution depends drastically on T_d and μ, and radiative transfer effects are much more important. When the latter are neglected, the lifetime against ionization that can be derived from upwind to downwind intensity ratio is grossly overestimated (Quémerais & Bertaux 1993), because there is an excess intensity in the downwind region in respect to the standard optically thin model that was often used up to now. A further complication is that there is some evidence from Voyager data that not all of this excess can be attributed to radiative transfer and therefore we have mainly focused on the upwind emission observations. Even in this case, several upwind D_∞ determinations which were based on overestimated lifetimes due to the downwind excess must be increased, according to the revised lifetime (Table 3). As mentioned earlier, for a given upwind intensity the product $D_\infty \times T_d$ is roughly constant for a certain μ.

The basis for the revised value of $T_d = 1.2 \times 10^6$ s comes both from an independent estimate based on direct solar wind measurements and EUV solar flux (Ajello et al. 1987), and from Lyα Voyager side view observations of the Maximum Emissivity Region, which lies at a few AU upwind from the Sun, and whose shape in the ecliptic plane can be directly and safely connected to the actual lifetime of H atoms (Lallement et al. 1991; Quémerais & Bertaux 1993). We also have added two new determinations of D_∞, from IUE observations (Clarke et al. 1984) and from a recent Hubble Space Telescope GHRS spectrum (Lallement et al. 1993).

Table 2 covers four different types of determinations :

1) The use of the instrument calibration at Lyα. This is the most common way. In principle one can distinguish between laboratory calibration and in-flight calibration on stars. The latter, in principle relatively precise, generally suffers from the required transformation from point sources to extended source emissions, which may involve imprecisely known instrumental parameters. In addition, the solar Lyα flux at line center must also be known.

2) The comparison with another Lyα extended source (geocorona, Venus-disk emission). This method has an additional model dependence through the calculation of this *auxiliary* source emission. However, the magnitude of this emis-

Table 2. Previous interplanetary H number density determinations.

Mission instrument	Year	I (Rayleigh) or initial D_∞ (cm^{-3})	T_d ($\times 10^6$ s)	method	reference
OGO-5	69-70	500-550 R (max)[2]		I. C.[1]	Thomas & Krassa (1974)
OGO-5	69-70	id.		I. C.	Bertaux & Blamont (1971)
Pioneer 10-11	72	350 R (max)		I. C.	Wu et al. (1981)
Pioneer 10-11	74	180 R (max)		I. C.	Wu et al. (1981)
Mariner 10	73-74	400 R (max)		I. C.	Broadfoot & Kumar (1978)
Prognoz	76-77	0.03-0.06 cm^{-3}	2-2.5	I. C.	Bertaux et al. (1985)
Pioneer-Venus	79-85	0.07-0.10 cm^{-3}(max)	1-1.2	I. C.	Ajello et al. (1987)
Pioneer-Venus	85-86	0.05 cm^{-3}(map)[3]	1.5	I. C.	Lallement & Stewart (1990)
Pioneer-Venus	86	0.08 cm^{-3}(max)	1-1.2	I. C.	Ajello (1990)
Voyager	77-83	0.30 cm^{-3}	1.2	I. C.	Lallement et al. (1990)
Galileo	90	0.07-0.10 cm^{-3}	2	I. C.	Pryor et al. (1992)
Galileo	90	0.16 cm^{-3}	1.4	I. C.	Ajello et al. (1993)
Copernicus	75	140-350 R (max)		Telescope[1]	Adams & Frisch (1977)
IUE	81-83	700-1000 R		Telescope	Clarke et al. (1984)
HST	91	500-600 R		Telescope	Lallement et al. (1993)
Voyager and SME	82	0.16 cm^{-3}		radiative transfer	Shemansky et al. (1984)
Pioneer 10 and SME	82	0.11 cm^{-3}		radiative transfer	Shemansky et al. (1984)
Venera 11-12	78-79	0.065 cm^{-3}	2	Venus Lyα	Chassefière et al. (1986)
Spacelab 1	83	750 R (max)		Geocorona	Bertaux et al. (1989)
Atlas 1 (ALAE)	92	0.165 cm^{-3}	1.1	Geocorona	(this work)
Ulysses (SWICS)	91	0.08 cm^{-3}	1.25	pick-up H^+	Gloeckler et al. (1993)

(1) Instrument Calibration and Telescope: the estimate of interplanetary Lyα emission and number density relies on instrumental calibration and knowledge of the solar flux.
(2) (max) means that the intensity measured near the upwind region was used.
(3) (map): the intensity was adjusted to fit a whole sky map, including both upwind and downwind region.

sion is in general rather well known because the H atmospheres have been studied by independent methods. This is the case of the present work, where knowledge of neither the instrument calibration nor the solar flux are necessary.

3) The use of the emission pattern through modeling of Lyman α radiative transfer effects. One can compare the solar Lyman α variation amplitudes (as directly measured from the Earth), and the reduced variations in the diffuse background observed by a distant spacecraft (Shemansky et al. 1984). The magnitude of the reduction depends on D_∞, as can be estimated from a full radiative transfer calculation.

4) The direct detection of a flow of *secondary* particles. Recently, H^+ pick-up ions resulting from charge exchange of neutral H atoms with solar protons have been detected by the SWICS instrument on board Ulysses (Gloeckler et al. 1993). Through modeling of their production rate between the Sun and the spacecraft, the neutral H number density can be estimated.

In Tables 2 and 3, the different observations have been sorted according to the four derivation methods listed above (We have put the telescope in a different category). The range of estimates is covered by the first group using instrument calibration. Uncertainties associated with imperfect modeling of the heliospheric density distribution (solar wind flux, solar Lyman α flux at line center, possible latitudinal variations of both of these parameters) might amount to an additional uncertainty of 20-30%. In the present exercise to re-derive D_∞ values, we have used a rather simple classical model with the relevant value of μ calculated for the epoch of observations and, except when stated otherwise, a mean lifetime of 1.2×10^6 s, with no solar wind latitude variations. From Table 2, it can be remarked that the lowest published densities are usually associated with a large lifetime T_d: 2-2.5 $\times 10^6$ s (Prognoz, Galileo, Pryor et al. 1992, Venera 11-12). Accordingly, the revised densities D_∞ indicated in Table 3 are higher by nearly a factor of 2.

The main conclusion from Table 3 is as follows: while the range of the total set of derived values, 0.035-0.30 cm^{-3}, (or 0.06-0.30 cm^{-3} without the very uncertain Copernicus value) is rather large, the 4 calibration-independent determinations result in the significantly narrower range 0.11-0.17 cm^{-3}. It would remain to explain why the scatter of D_∞ values derived from instrument calibration is so large, though most of them had the opportunity to check, re-assess and modify their laboratory

Table 3. Revised H number density.

Mission instrument	Year	H lifetime at 1 AU ($\times 10^6$ s)	D_∞ (cm^{-3})	revised in this work
OGO-5	69-70	1.2	0.10-0.11 cm^{-3}	yes
Pioneer 10-11	72	1.2	0.09 cm^{-3}	yes
Pioneer 10-11	74	1.2	0.11 cm^{-3}	yes
Mariner 10	73-74	1.2	0.10 cm^{-3}	yes
Prognoz	76-77	1-1.2	0.06-0.12 cm^{-3}	yes
Pioneer-Venus	79-85	1-1.2	0.07-0.10 cm^{-3}	no
Pioneer-Venus	85-86	1-1.2	0.07-0.08 cm^{-3}	yes
Pioneer-Venus	86	1-1.2	0.08 cm^{-3}	no
Voyager	77-83	1-1.2	0.23-0.3 cm^{-3}	no
Galileo	90	1.2	0.16 cm^{-3}	yes
Galileo	90	1.4	0.16 cm^{-3}	no
Copernicus	75	1.2	0.035-0.09 cm^{-3}	yes
IUE	81-83	1.2	0.13-0.17 cm^{-3}	yes
HST	91	1.2	0.11-0.13 cm^{-3}	yes
Voyager/SME	82	N.A.	0.16 cm^{-3}	no
Pioneer/SME	82	N.A.	0.11 cm^{-3}	no
Venera 11-12	78-79	1.3	0.11 cm^{-3}	yes
Spacelab 1	83	1.2	0.17 cm^{-3}	yes
Atlas 1 (ALAE)	92	1.1	0.165 cm^{-3}	yes

N.A. : not applicable

based calibrations with hot stars observations emitting a continuum around 120-130 nm. In this respect it might be interesting to note that the IUE and GHRS/HST telescope measurements seem to agree reasonably well with the calibration independent results, possibly owing to a better knowledge of their very small field-of-view.

8. Conclusion

From the present work on the ALAE data and from the clustering of D_∞ determinations by instrument calibration independent methods, it seems now firmly established that the density of neutral H at $\approx$ 50 AU upwind is within the range of values defined by 0.135 ± 0.025 cm^{-3}. This is nearly a factor of two higher than earlier determinations derived from observations in the 70's, but this discrepancy can be explained mainly by the use of an erroneous lifetime T_d of H atoms in the early modeling efforts, induced by an incorrect interpretation of upwind to downwind intensity ratio.

Such a relatively high value of D_∞ is important for our understanding of the physical conditions in the outer heliosphere and in the interstellar medium. First, let us remember that in the case of a strong plasma interaction at the heliopause, the interstellar hydrogen flow may be filtrated through charge exchange coupling with the decelerated protons of the solar wind, thus creating a strong gradient of hydrogen density (Baranov et al. 1991). In such a case, the value of D_∞ determined in this work applies only to the conditions of the flow after crossing the heliopause. The actual value of the hydrogen number density in the interstellar medium is then higher than D_∞ but cannot be determined from the Lyα glow pattern seen from Earth's orbit.

The increase of the estimate of the value of D_∞ by a factor of two gives more weight to the hypothesis of a strong shock at the heliopause. For a given ionization ratio in the interstellar medium, we find twice as many interstellar protons than earlier estimates. Consequently, the larger dynamic pressure of the interstellar flow would push the contact discontinuity closer to the Sun. Then, the heliopause could be closer (within 100 AU) than usually estimated.

Acknowledgements. The authors are greatly indebted to the various people who have helped during the ATLAS 1 mission preparation, flight, and subsequent data analysis. Among them, we wish to thank ALAE co-investigator Dr. Gaston Kockarts who has provided advice and implemented the MSIS model at Service d'Aéronomie and Dr. Florence Goutail for her dedication to the calibration and flight operations. The data acquisition has been made possible by the activity of the people of the Marshall Space Flight Center, of the ATLAS 1 mission scientist Dr. Marsha Torr and of the astronauts aboard the shuttle. We wish to thank also ALAE project manager Emmanuel Dimarellis for his spectacular achievement of a flawless mission, Christian Taulemesse for designing the optics, Christian Bernard for the fabrication of H and D cells, Frantz Semelin for the electronics and Jean-Claude Lebrun for data processing. All are CNRS personnel at Service d'Aéronomie and additional financial support was provided by CNES. We also wish to

thank the ESA support team on the ground and, in space, the belgian astronaut Dirk Frimout who helped the ALAE flight operations.

References

Adams T.F., P.C. Frisch 1977, ApJ, 212, 300
Ajello J.M, Stewart A.I., Thomas G.E. & Graps A. 1987, ApJ, 317,964
Ajello J.M., JGR, 95, A9, 14855, 1990.
Ajello J.M., Pryor W.R., Barth C.A., Hord C.W., Simmons K.E. 1993, Adv. Space Res., 13, (6), 37
Banks P.M., Kockarts G. 1973, Aeronomy, Academic press, New York
Baranov V.B., Lebedev M.G. & Malama Y.G. 1991, ApJ, 375, 347
Baranov V.B., Malama Y.G. 1993, JGR 98, A9, 15157
Bertaux J.L., Blamont J.E. 1971, A & A 11, 200
Bertaux J.L., Lallement R., Kurt V.G. & Mironova E.N. 1985, A & A 150, 1
Bertaux J.L., Le Texier H., Kockarts G., Dimarellis E., Goutail F., 1989, Annales Geophysicae, 7, (6), 549
Bertaux J.L., Quémerais E., Goutail G., Kockarts G., Sandel B.R. 1992, GRL, 20, (6), 507
Broadfoot A.L., Kumar S. 1978, ApJ., 222, 1054
Chassefière E., J.L. Bertaux, R. Lallement, V.G. Kurt 1986, A & A, 160, 229
Clarke J.T., S. Bowyer, H.J. Fahr , G. Lay 1984, A & A, 139, 389
Gloeckler G., Geiss J., Balsiger H., Fisk L.A., Galvin A.B., Ipavich F.M., Ogilvie K.W., Steiger R., Wilken B., Science, 261, July 2, 1993
Hedin A. 1983, JGR, 88, A12, 10170
Lallement R., Bertaux J.L., Dalaudier F. 1985, A & A, 150, 21
Lallement R., J.L. Bertaux, V.G. Kurt 1985, JGR, 90, A2, 1413
Lallement R., I. A. Stewart 1990, A & A, 227, 608
Lallement R., Bertaux J.L., Chassefière E. and Sandel B.R. 1991, A & A, 252, 385
Lallement R., Bertaux J.L., Clarke J.T., Science, May 21, 1993.
Lean J. 1990, JGR, 95, 11933
Meier R.R. 1991, Space Science Reviews 58,1/2
Osterbart R., Fahr H.J. 1992, A & A, 264, 260
Pryor W.R., Ajello J.M., Barth C.A., Hord C.W., Stewart A.I., Simmons K.E., McClintock W.E., Sandel B.R., Shemansky D.E. 1992, ApJ, 394, 363
Quémerais E. 1993, Thèse de doctorat de l'université Paris 6
Quémerais E., Bertaux J.L. 1993, A & A, 277, 283
Shemansky D.E., Judge D.L., Jessen J.M. 1984, in Local Interstellar Medium , IAU Colloquium, Nasa CP-2345
Thomas G.E. 1963, JGR, 68, 2639
Thomas G.E., Krassa R.F. 1971, ApJ, 134, 20
Thomas G.E., R.F. Krassa 1974, A & A, 30, 223
Thomas G.E. 1978, Ann. Rev. Earth Planet. Sci. 6, 173
Wu F.M., Suzuki K., Carlson R.W. and Judge D.L. 1981, ApJ., 245, 1145

This article was processed by the author using Springer-Verlag LaTeX A&A style file version 3.